CFD Letters

Journal homepage:
https://semarakilmu.com.my/journals/index.php/CFD_Letters/index
ISSN: 2180-1363

Numerical Study of Shear and Extensional Inelastic Contraction Flows

Alaa Abdulwahid Sharhan[1,*], Alaa H. Al-Muslimawi[1]

[1] Department of Mathematics, College of Science, University of Basrah, Basrah-61004 Iraq

ARTICLE INFO

Article history:
Received 2 February 2023
Received in revised form 5 March 2023
Accepted 4 April 2023
Available online 1 August 2023

Keywords:
Contraction flows; Inelastic fluid; Taylor Galerkin method; shear viscosity; extensional viscosity

ABSTRACT

This study investigates the numerical solution of viscous sharp contraction flow using a time-step Taylor-Galerkin-pressure correction finite element method (T-G/P-C). Such a complex problfem displays a start-up, 4:1contraction creeping flow, shear viscosity and extensional viscosity responses. Here, inelastic shear-extensional viscosity model is proposed with a single power-index response and identical in shear and extension, namely Fit-I. In this context, extension rate and shear rate are defined by depending on the second and third invariants of the rate of deformation tensor. Employing (T-G/P-C) method by combining with extensional and shear viscosity representation to treat such problem gives novel scenario. The interesting of this study lies in determining the efficient effect of relevant parameters of inelastic shear-extensional viscosity model on the solutions components, and rate of convergence issues. Attention also is paid to the impact of these parameters on the rate of convergence issues.

1. Introduction

Non-Newtonian fluids play an important role in many chemical and industrial processes encountered in polymers, minerals, foods, and biological industries. In this type of fluid, the viscosity changes under the forces of stress. Thus, for that purpose fundamental constitutive equation is used to describe the viscosity of such fluid. Typical constitutive models to display the non-Newtonian behavior are power law, modified power law, Herschel–Bulkley model, cross model, Carreau model, Bird-Carreau, Carreau-Yasuda, Binding Model and Modified Casson [1-5]. Further, the non-Newtonian fluids display either shear-thinning (viscosity decrease as shear increases) or shear thickening (viscosity increases as shear increases) natures.

In the present work we explore inelastic fluid flow response. Thus, one of the most fundamental constitutive equations for such fluids, which depicts the shear viscosity and extensional viscosity responses is employed; called Fit I-model. Some details of this model are provided by Binding *et al.,* [6] and Debbaut and Crochet [7]. Where the definition of shear and extensional viscosity is

$$\mu_s(\dot{\gamma}) = \mu_0(1 + (k\dot{\gamma})^2)^{(n-1)/2}$$

* *Corresponding author.*
E-mail address: eala.khashab.sci@uobasrah.edu.iq (Alaa Abdulwahid Sharhan)

https://doi.org/10.37934/cfdl.15.8.107121

$$\mu_E(\dot{\varepsilon}) = 3\mu_0 \, cosh(n\lambda\dot{\varepsilon}) \, . \, (1 + 3(k\dot{\varepsilon})^2)^{(n-1)/2} \, ,$$

where n, λ and k are the parameters that determine the shear and extensional components in the model and μ_0 represents the zero-shear viscosity [6-10]. In general, this model represents functional form of the viscosity in combined shear and extensional flows. Several researchers, like Binding, Debbaut, and Al-Muslimawi, have done studies on this model that show how useful it is and how it can solve and answer questions about flows with shear viscosity and extension viscosity. The study makes use of a model that describes the shear and extensional behaviors of the fluid. Currently, there is no recognized constitutive theory to characterize the influence of shear and extensional viscous on complex inelastic flows. Consequently, a realistic strategy is needed. When the flow is steady and there is just one shear, we express the viscosity as $\mu_s(\dot{\gamma})$ with the shear rate $(\dot{\gamma})$ and depending on the extension rate $(\dot{\varepsilon})$, the extensional viscosity is defined in a uniaxial flow as $\mu_E(\dot{\varepsilon})$. When calculating shear viscosity, rheumatic studies are often used, although the measurement of extensional viscosity in practice is a greater challenge. Diagnostics of shear and extensional viscosity have been proposed using a variety of techniques, some more complex than others [6,7]. The material behavior in these straightforward flows must be described by any model that tries to characterize the additive extension and shear influence on fluid viscosity. It is hoped that for complicated flows, including both shear and extension, such a model would also be able to maintain intricate modelling of fluid flow. The main novelty in this research is the study of the effect of the parameters variation of this model during fluid flow in a 4:1 contraction channel, which none of the researchers previously shed light on. The numerical approach utilized here is a time-marching (T-G/P-C) finite element method, which was previously suggested by Hawken *et al.,* [11]. This numerical algorithm is derived based on a temporal Taylor series expansion and a two-step Lax-Wendroff time-stepping procedure. This method is successfully applied in a number of various flow situations [12]. Following that, (T-G/P-C) approach is used for more complicated problems including inelastic flows, both with and without viscous heating effects, in order to get more accurate solutions. Briefly, the algorithm is that combines Taylor Galerkin schemes with a pressure-correction scheme. Taylor-Galerkin techniques are recommended for efficiently resolving convection-diffusion problems, while the pressure correction approach incorporates the incompressibility restriction through fractional stages. This results in a pair of predictor-corrector equations, with the diffusion terms addressed in a Crank-Nicolson method and the convection terms treated explicitly or implicitly [13]. Several studies of axisymmetric contraction flows have been published [14-16]. This is mostly due to the fact that the contraction results in spatially complicated flow profiles, which are difficult to estimate numerically when the contraction occurs. In this work, we use (T-G/P-C) finite element method with an upwind strategy to approximation terms to represent non-Newtonian (inelastic) flows in abrupt axisymmetric 4:1 contraction. The goal of the research is to look at the different impacts of variation on parameters viscosity model. The novelty of this study is in the application of this new viscosity model to the study of inelastic fluid flow via a 4:1 abrupt contraction channel using the (T-G/P-C) technique. In the following section the governing equations of non-Newtonian fluid is provided in the cylindrical coordinate format. The numerical approach is presented in Section 3. The problem specification and numerical results are discussed in details in Sections 4 and 5.

2. Methodology

2.1 Mathematical Modeling

The differential equations that govern isothermal incompressible inelastic flow consist of the continuity and momentum equations, which are given with the absence of body forces in following forms [17]:

$$\nabla \cdot u = 0, \tag{1}$$

$$\rho\left(\frac{\partial u}{\partial t} + u \cdot \nabla u\right) = -\nabla p + \nabla \cdot (2\mu_s(\dot{\gamma}, \dot{\varepsilon})d), \tag{2}$$

where *u*, *p* and *ρ* represent the fluid velocity, hydrodynamic pressure and density. In addition, $d = \frac{1}{2}(\nabla u + \nabla u^{\tau})$ is the deformation rate and ∇ is the gradient operator. Moreover, the non-dimensional group of Reynolds number may be defined by the scaling $Re = \rho\frac{UL}{\mu}$, in which, *(ρ), (U), (L)* and *μ* are density, characteristic velocity, length scale, and viscosity, respectively. Therefore, the momentum equation can be given in non-dimensional form as follows:

$$Re\frac{\partial u}{\partial t} = \nabla \cdot (2\mu(\dot{\gamma}, \dot{\varepsilon})d) - Re(u.\nabla u) - \nabla p. \tag{3}$$

Also, the shear rate $\dot{\gamma}$ and strain rate $\dot{\varepsilon}$ of simple shear flow and extensional flow are represented by:

$$\begin{aligned} \dot{\gamma} &= 2\sqrt{II_d} \\ \dot{\varepsilon} &= 3\frac{III_d}{II_d} \end{aligned}, \tag{4}$$

In an axisymmetric coordinate system, II_d and III_d are the second and third invariants of the rate of strain tensor, which may be described as follows [18,19]:

$$II_d = \frac{1}{2}\mathrm{tr}(d^2) = \frac{1}{2}\left\{\left(\frac{\partial u_r}{\partial r}\right)^2 + \left(\frac{\partial u_z}{\partial z}\right)^2 + \left(\frac{u_r}{r}\right)^2 + \frac{1}{2}\left(\frac{\partial u_r}{\partial z} + \frac{\partial u_z}{\partial r}\right)^2\right\}. \tag{5}$$

And,

$$III_d = \det(d) = \frac{u_r}{r}\left\{\frac{\partial u_r}{\partial r}\frac{\partial u_z}{\partial z} - \frac{1}{4}\left(\frac{\partial u_r}{\partial z} + \frac{\partial u_z}{\partial r}\right)^2\right\}. \tag{6}$$

In this study inelastic shear-extensional viscosity model is assumed, namely Fit-I, with the following material functions [6]:

$$\begin{aligned} \mu_s(\dot{\gamma}) &= \mu_0(1 + (k\,\dot{\gamma})^2)^{(n-1)/2} \\ \mu_E(\dot{\varepsilon}) &= 3\mu_0\cosh(n\lambda\dot{\varepsilon}).(1 + 3(k\,\dot{\varepsilon})^2)^{(n-1)/2} \end{aligned}, \tag{7}$$

where, μ_0 is zero shear viscosity is a consistency parameter and *n* is the power index of the fluid, *k* is the natural time constant (unrelated to fluid elasticity), and λ is constant for the fluid.

2.2 Numerical Method

A semi-implicit time-stepping (T-G/P-C) scheme is utilized to treat the relevant differential equations. This method is a fractional step approach that discretized first in the temporal domain, utilizing Taylor series expansions in time, then a pressure-correction procedure to extract a time stepping scheme of second-order accuracy. The flow domain is assumed to be discretized into a triangle mesh, with piecewise continuous linear (pressure) and quadratic (velocity) interpolation functions applied to such constituent sections. Per time step, the Taylor-Galerkin algorithm comprises three separate fractional stages:

Stage 1: A two-step predictor-corrector approach is used to compute non-divergence-free $u^{n+1/2}$ and *u** fields given starting velocity and pressure fields.

Stage 2: Calculate the pressure difference ($p^{n+1} - p^n$) using *u** and the Poisson equation based on the Choleski technique.

Stage 3: By Jacobi iteration, we find a divergence-free velocity field u^{n+1} using *u** and the pressure difference ($p^{n+1} - p^n$).

Now the three stages within each time-step are represented mathematically as follows:

Step 1a: $[\frac{2Re}{\Delta t}M + \frac{1}{2}S](U^{n+\frac{1}{2}} - U^n) = \{-[S + \rho N(U)]U + L^T P\}^n,$ (8)

Step 1b: $[\frac{Re}{\Delta t}M + \frac{1}{2}S](U^* - U^n) = \{-SU + L^T p\}^n - \rho[N(U)U]^{n+\frac{1}{2}},$ (9)

Step 2: $K(P^{n+1} - P^n) = -\frac{Re}{\theta \Delta t}LU^*,$ (10)

Step 3: $\frac{Re}{\Delta t}M(U^{n+1} - U^*) = \theta L^T(P^{n+1} - P^n).$ (11)

The matrices *M, S, N, K* and L indicate the mass, momentum diffusion, convection matrix, pressure stiffness matrix and divergence/pressure gradient, respectively, of the system [20-23]. Such that

$$M_{ij} = \int_\Omega \phi_i \phi_j d\Omega, \quad K_{ij} = \int_\Omega \nabla\psi_i \nabla\psi_j d\Omega, \quad N(U)_{ij} = \int_\Omega \phi_i (U^n . \nabla\phi_j) d\Omega$$

$$(L)_{ij} = \int_\Omega \psi_i (\nabla . \phi_j)\, d\Omega, \quad (S)_{ij} = \int_\Omega \mu_s(\dot{\gamma}.\dot{\varepsilon})\left[\nabla\phi_i : \nabla\phi_j + (\nabla\phi_j)^\tau\right] d\Omega$$

2.3 Problem Specification and Boundary Conditions

In the present work we used 4:1 axisymmetric sharp contraction channel as benchmark problem. For that purpose, a fine mesh (FM) is constructed, with a geometric schematic and mesh ingredients are shown in Figure 1(a) and Table 1, respectively.

Boundary conditions (BCs): For the present channel issue, the BC configuration is as follows:

(i) At the inlet, the flow is characterized as Poiseuille (*Ps*) flow with zero radial velocity.
(ii) On the bottom walls of the channel, no-slip *BCs* are installed.
(iii) At the axisymmetric line of channel, zero radial velocity is applied.
(iv) For outlet, there is no pressure and the radial velocity of the axisymmetric line is zero.

Figure 1(b) depicts a visual representation of all that has been spoken above.

Table 1
Mesh characteristics

Mesh	Total Elements	Total Nodes	Boundary Nodes	Pressure Nodes
MF	1128	2387	244	639

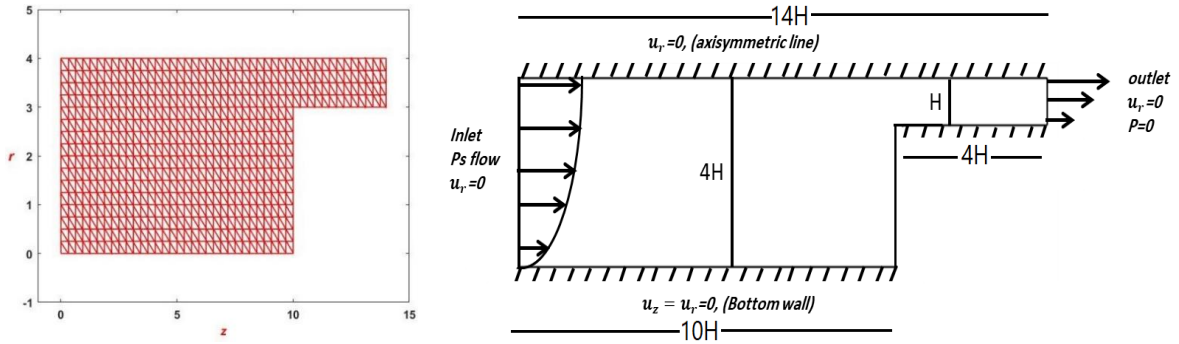

(a) (b)

Fig. 1. (a) Structured finite element mesh, (b) Flow geometry

3. Results

The numerical solutions concerned with the rate of error convergence for inelastic flows through an axisymmetric 4:1 contraction channel (Figure 1(a)) by using (T-G/P-C) finite element method. The effect of various parameter of inelastic shear-extensional viscosity model such as zero shear viscosity (μ_0), power index (*n*), natural time constant (*k*) and constant for the fluid (λ) is conducted.

3.1 Shear Viscosity

***k*-variation:** The rate of convergence of axial velocity and pressure is shown clearly in Figure 2 and Figure 3, respectively, for fixed {*Re*=10, $\mu_0 = 2$ } and *k* variation in both shear thinning (*n*=0.8) and shear thickening (*n*=2.8) cases. Generally, the results reveal that, increasing *k* leads to decrease in the level of convergence rate with significant increasing for shear thickening case, while increasing *k* in shear thinning leads to an increase in convergence rate. Meaning, the convergence to the steady-state is monitored as *k*, increasing where in the shear thinning case more time is needed to get the converged solution (see Figure 2(a)), while an opposite feature is noticed for shear thickening cases (see Figure 2(b)). For instance, with *k*=10, the level of time in the shear thickening cases is much less than that in the shear thinning case (needed around 16 for shear thinning cases compared to 8 for shear thickening).

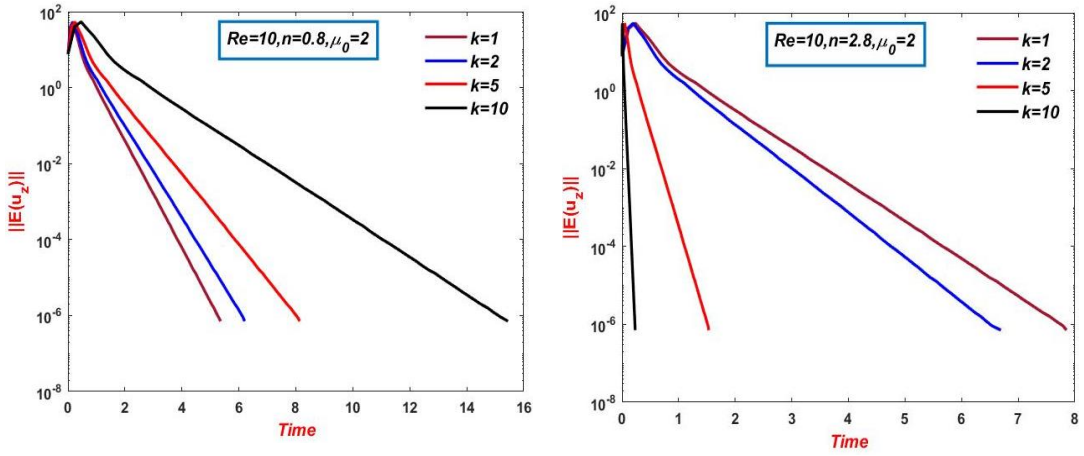

(a) (b)

Fig. 2. Convergence of velocity; *k* variation, μ_0=2, *Re*=10, *(a) n*=0.8, *(b) n*=2.8

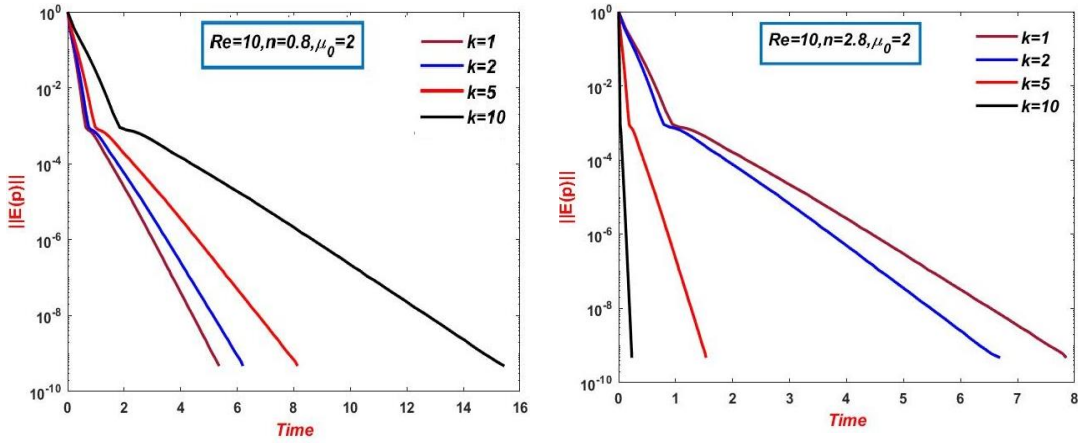

(a) (b)

Fig. 3. Convergence of pressure; *k* variation, μ_0=2, *Re*=10, (a) *n*=0.8, (b) *n*=2.8

n-variation: Figure 4(a) and Figure 4(b) depict the rate of axial velocity convergence in both shear thinning and shear thickening, respectively, while the Figure 5(a) and Figure 5(b) display the rate of pressure convergence, for fixed {*Re*=10, *k*=1, $\mu_0 = 2$}. From the profiles one can observed that, increase in *n* leads to reduction in the time when *n* <1 (Figure 4(a) and Figure 5(a)), while the relationship between time and *n* is an inverse relationship for *n* >1 (Figure 4(b) and Figure 5(b)). The contrary will be seen in the case of shear thickening; possibly this is due to the fluids behaving in a different way. In addition, in the case of *n* =1, less time is taken to reach to the ideal solution because this level of *n* is far from the critical values of *n*. This means that the Newtonian fluid takes less time to get the converge results compared to the inelastic fluid. We also can see this hold for the inelastic power law model [18,24]. For clear feature, more details about the relationship between the power index *n* and the time are illustrated in Figure 6.

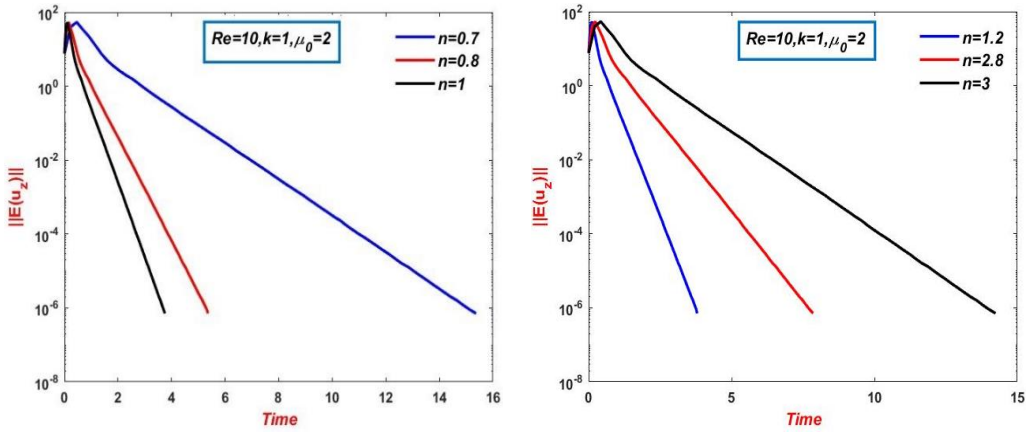

(a) (b)

Fig. 4. Convergence of velocity; *n* variation, μ_0=2, *Re*=10, *k*=1, (a) *n*<1, (b) *n*>1

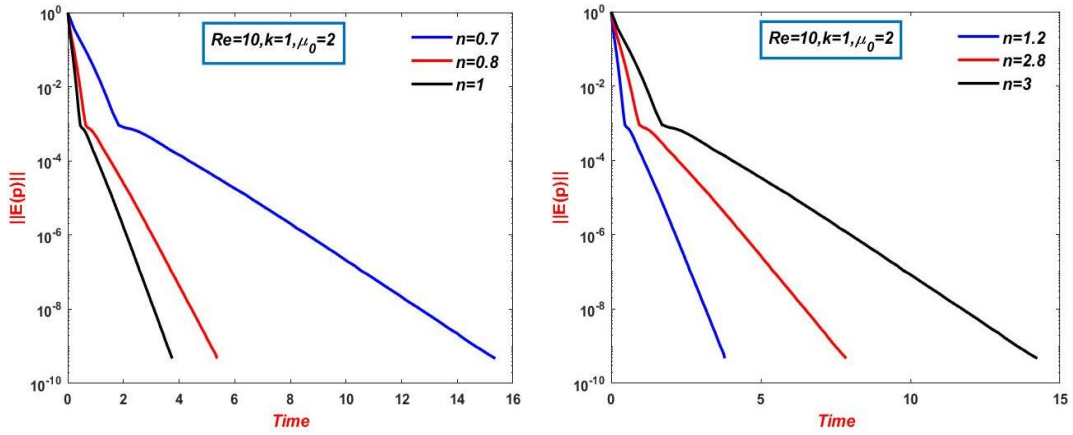

(a) (b)

Fig. 5. Convergence of pressure; *n* variation, μ_0=2, *Re*=10, *k*=1, (a) *n*=0.8, (b) *n*=3

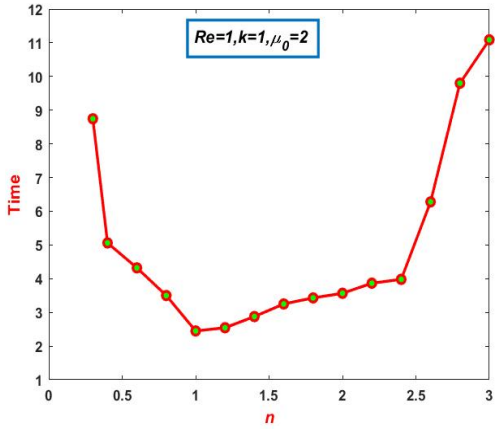

Fig. 6. Power index (*n*) vs. time with *Re*=1, *k*=1, μ_0=2

The relationship between maximum axial velocity and power index *n* in shear thinning and shear thickening, respectively with fixed {*Re*=1, *k*=1, μ_0=2} is presented in Figure 7(a) and Figure 7(b). In both cases a direct proportionality between the maximum velocity and *n* is occurred with high level is appeared in the shear thickening situation, which is consistence with findings reported by others in power law model too [25].

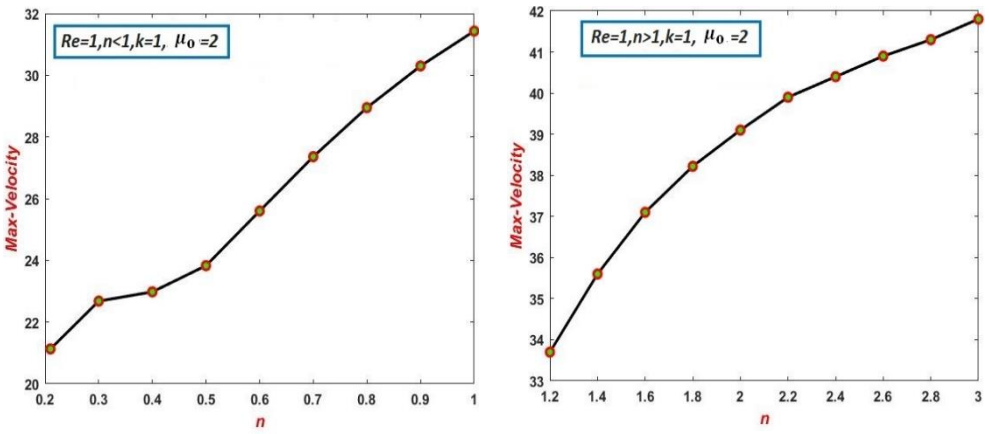

(a) (b)

Fig. 7. Increasing correlation between *n* and maximum velocity with: *Re*=1*, k*=1*,* μ_0=2*, (a) n*<1, (b) *n*>1

μ_0-variation: The history convergence tolerances of axial velocity and pressure with μ_0 variation and {*Re*=10 and *k* =1} are shown in Figure 8 and Figure 9 again in shear thinning *(n*=0.8*)* and shear thickening (*n*=2. 8). In general, for velocity and pressure we observed that raising μ_0 generates a decreasing in the rate of convergence, in both cases shear thinning and shear thickening. As the value of (μ_0) in this model approaches zero, it gets closer to its critical value. It has been shown that the time required to obtain convergence increases as the parameters approach their critical values. So, as we can see in Figure 8, the time needed to obtain convergence increases as (μ_0) decreases.

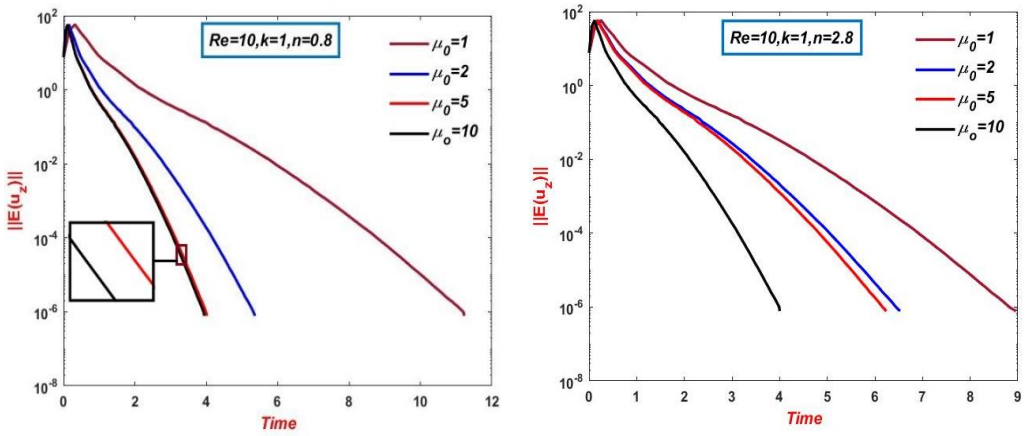

(a) (b)

Fig. 8. Convergence of velocity; μ_0 variation, *k*=1*, Re*=10, (a) *n*=0.8, (b) *n*=2.8

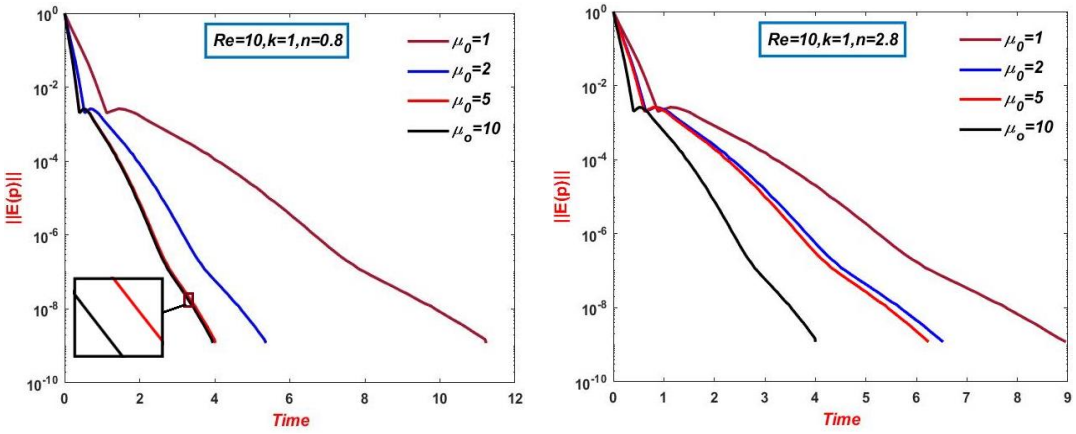

(a) (b)

Fig. 9. Convergence of pressure; μ_0 variation, *k*=1, *Re*=10, (a) *n*=0.8, (b) *n*=2.8

***Re-variation*:** Figure 10 and Figure 11 demonstrate the rate of convergence of axial velocity and pressure for fixed {*k*=1, μ_0=2} and *Re*-variation in both shear thinning and shear thickening cases. Findings show that raising *Re* causes a significant increase in the level of convergence rate for both situations, which reflects the difficulties of convergence for large Re number. For instance, for axial velocity when Re = 2, the level of time is much less than that in Re = 20 (around three times lee than) ((see Figure 10(a) and Figure 10(b)). Once more, these results are consistent with the findings of others.

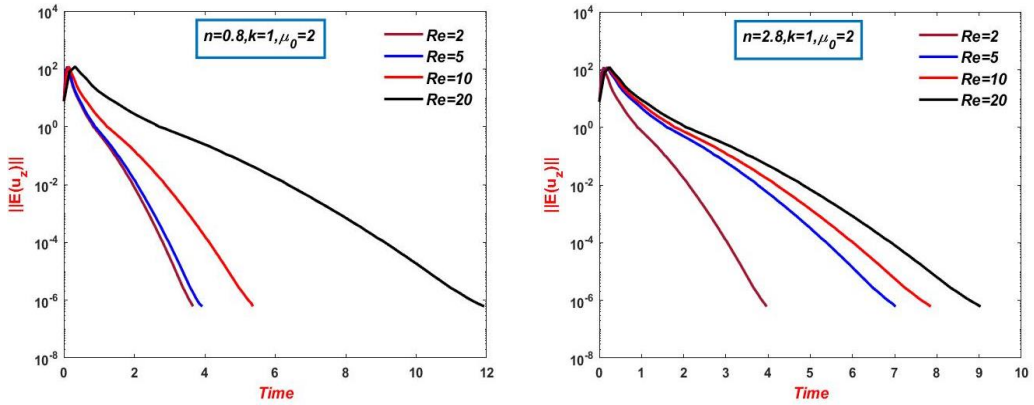

(a) (b)

Fig. 10. Convergence of velocity; *Re* variation, μ_0 =2, *k*=1, (a) *n*=0.8, (b) *n*=2.8

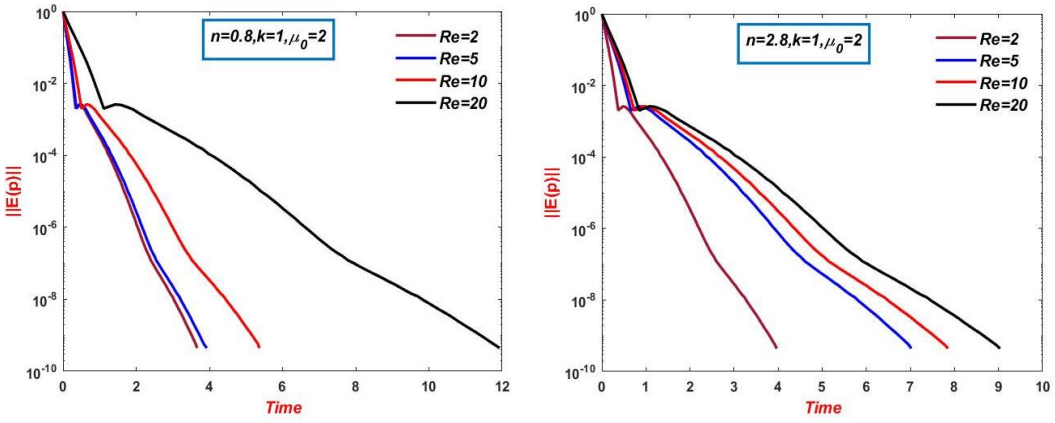

(a) (b)

Fig. 11. Convergence of pressure; *Re* variation, μ_0 =2, *k*=1, (a) *n*=0.8, (b) *n*=2.8

3.2 Extensional Viscosity

***k-variation*:** For *k* variation {0.01, 0.05, 0.1, 0.5}, Figure 12(a) and Figure 12(b) show the rate of axial velocity convergence *n*<1, (*n*=0.8) and *n>1*, (*n* =1.6), with fixed {*Re*=10, λ =0.1, *k*=1, μ_0=2} and. In addition, with a same situation the convergence level of pressure is presented in Figure 13(a) and Figure 13(b). Actually, the findings reveal that, in the case of *n*<1 there is a significant effect of *k* on the level of convergence of both velocity and pressure, where the rate of convergence increases as *k* raised. In contrast, in *n>1* situation an opposite feature is appeared with modest change, in which the level of convergence inversely correlated with the time. For more details on the rate of convergence in *k*-variation, see section 5.1 (*k*-variation) for details on this.

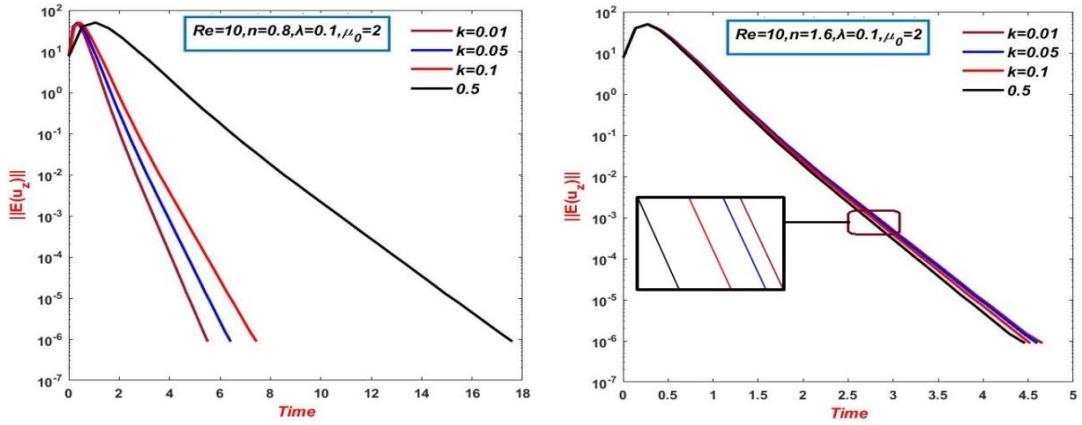

(a) (b)

Fig. 12. Convergence of velocity; *k* variation, μ_0 =2, λ =*0.1*, *Re* =10*,* (a) *n=0.*8, (b) *n*=2.8

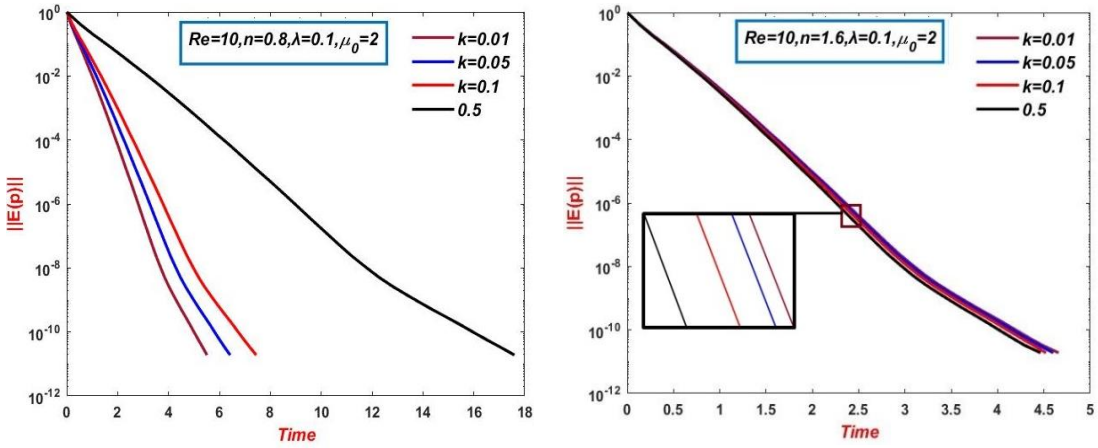

(a) (b)

Fig. 13. Convergence of velocity; *k* variation, μ_0 =2, λ =*0.1*, *Re* =10*,* (a) *n=0.*8, (b) *n*=2.8

λ-variation: Again, in both cases of n<1, (*n* =0.8) and *n*>1*,* (*n* =1.6), the rate of convergence of velocity and pressure with fixed {*Re*=10*, k* = 0.01*,* μ_0 =2} and λ variation {0.05,0.08,0.1,0.2} is presented in Figure 14 and Figure 15. Generally, same level of convergence is occurred for velocity and pressure in both cases n<1 and n>1. In addition, the rate of convergence level of velocity and pressure is decreased as the level of λ reduced, with high level in the *n*>1 situation. As the value of λ is increased, it gets closer to its critical value, and it takes more time to reach the error stopping criterion ($E = 10^{-6}$).

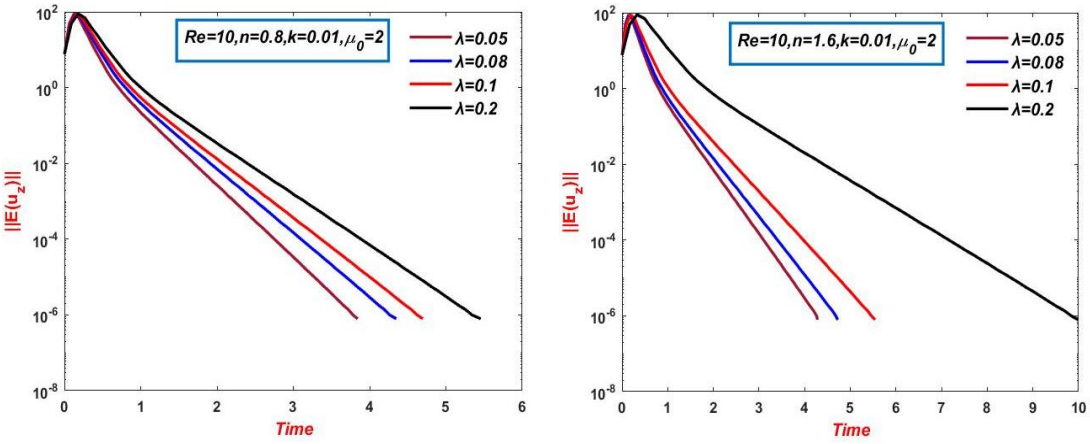

(a) (b)

Fig. 14. Convergence of velocity; λ variation, *k*=0.01, μ_0 =2, *Re*=10, *(a) n*=0.8, *(b) n*=1,6

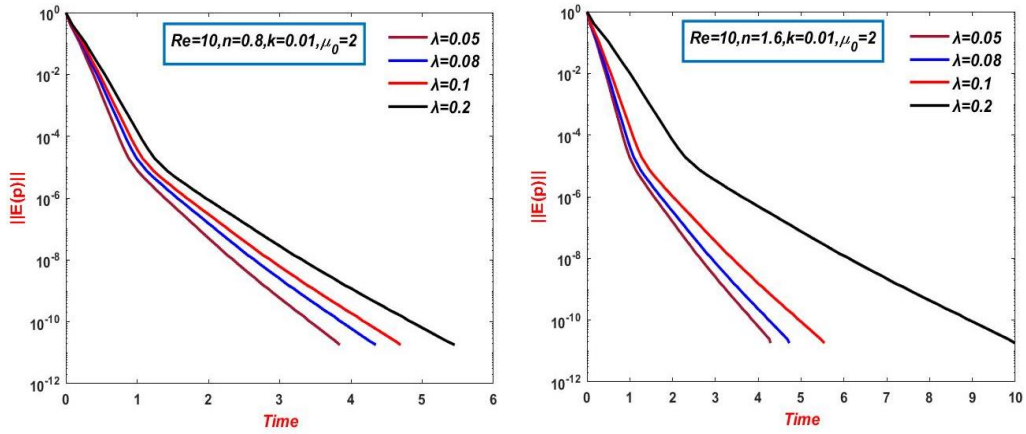

(a) (b)

Fig. 15. Convergence of pressure; λ variation, *k*=0.01, μ_0 =2, *Re*=10, (a) *n*=0.8, (b) *n*=1,6

n-variation: The influence of power index (*n*) on the velocity and pressure convergence is illustrated in Figure 16 and Figure 17, respectively, at {*Re* = 10, *k* = 0.1, λ = 0.1, μ_0 = 2}. Here, two different setting of power index (*n*) are presented, when *n*<1 for *n*= {0.6, 0.8, 1}and *n*>1 for *n*= {1.6, 2, 2.4}. In both cases, the direct relationship between *n* and the time represents an essential point in this manner, where an increase in the value of *n* results an increase in the time. That the rate of convergence in shear thickening situation is about twice of that in shear thinning case. This is due mathematically to the extra term (hyperbolic function (*cosh*)) in the extensional viscosity dependence.

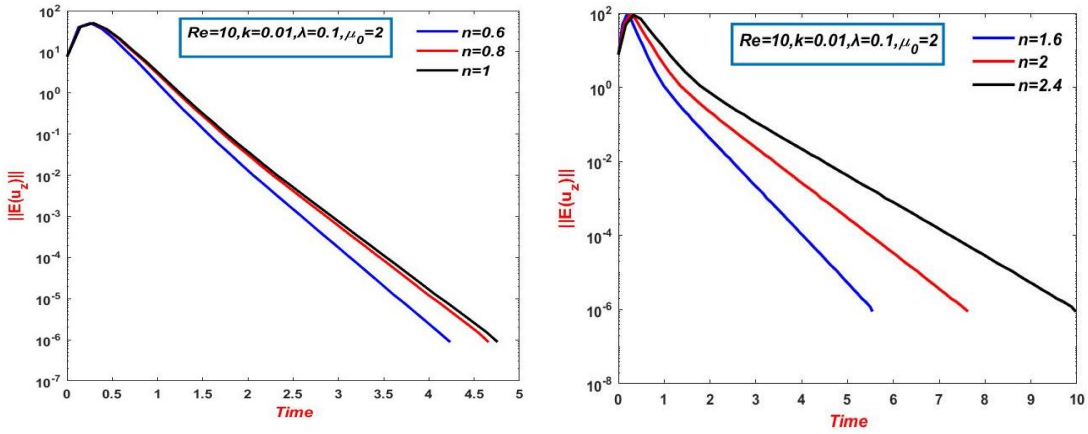

(a) (b)

Fig. 16. Convergence of velocity; *n* variation, μ_0=2, *Re*=10, *k*=0.01, λ =0.1 (a*) n*<1, (b) *n*>1

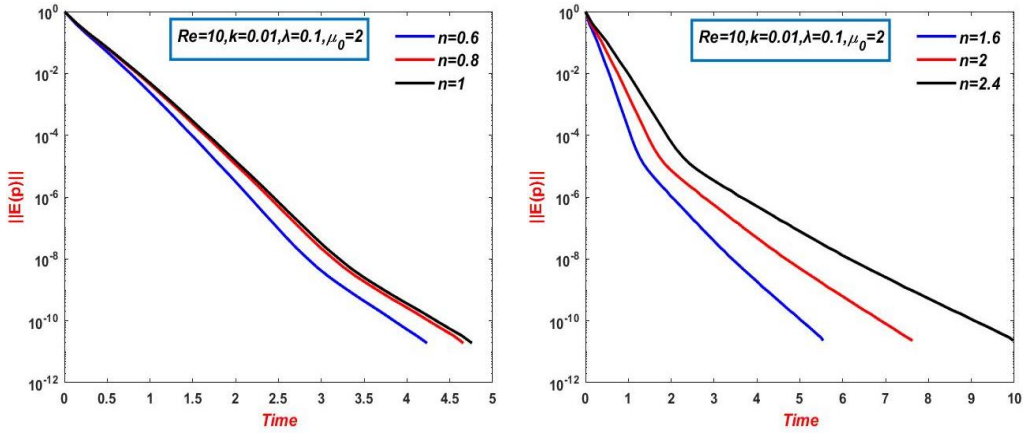

(a) (b)

Fig. 17. Convergence of pressure; *n* variation, μ_0=2, *Re*=10, *k*=0.01, λ =0.1 (a*) n*<1, (b) *n*>1

For more clarification, the relation between the power index *n* and the time is shown in Figure 18 for {*Re*=1*, k*=0.01*,* λ =0.1 and μ_0=2}. The profile provides clear feature of the effect of *n* on the time, where it is clear that increasing *n* generates an increase in the time. As anticipated, the profile provides clear feature of the effect of *n* on the time, where it is clear that increasing *n* generates an increase in the time, which is consistent with the results found by others. Addition, the results reflect one of the most important difficulties in the simulation that researchers face in the case of shear thickening (when *n*>1), where they need long time to get the steady solutions compared to shear thinning cases. Maximum velocities are shown to decrease as *n* increases (see Figure 19).

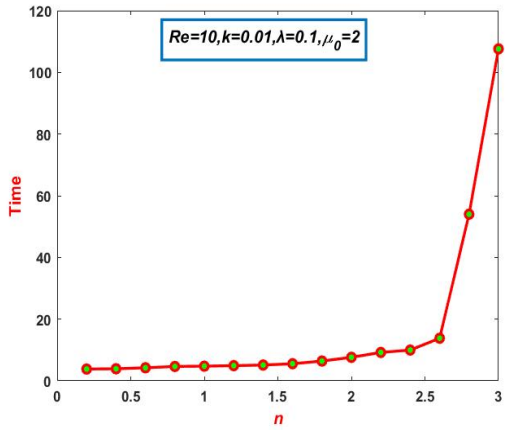

Fig. 18. *n* vs. time with *Re*=1, *k*=0.01, λ =0.1 and μ_0=2

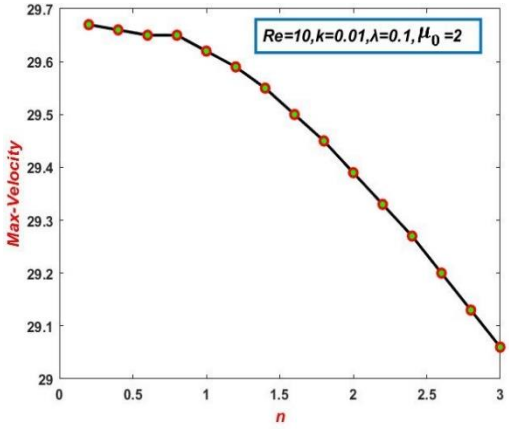

Fig. 19. Maximum velocity as function of *n* with *Re*=1, λ =0.1, *k*=1, μ_0=2

μ_0-variation and Re-variation: For more discussion, the simulation has been done for variation of zero shear viscosity. Here, velocity and pressure convergence histories for constant parameter-setting with {*Re*=10, *k*=0.01, λ =0.1} and variation μ_0={0.5,1,2,3} are presented in Figure 20 and Figure 21 for both cases when n<1, (*n*=0.8) and n>1, (*n =1.6*). The findings reveal that, for both *n*>1 and *n*<1 an inverse relationship between the zero-shear viscosity and rate of convergence of velocity and pressure. So, one may observe that increases the level of zero shear viscosity is led to reduce the level of simulation time. In addition, we found same results and trend for the variation in *Re* (not shown).

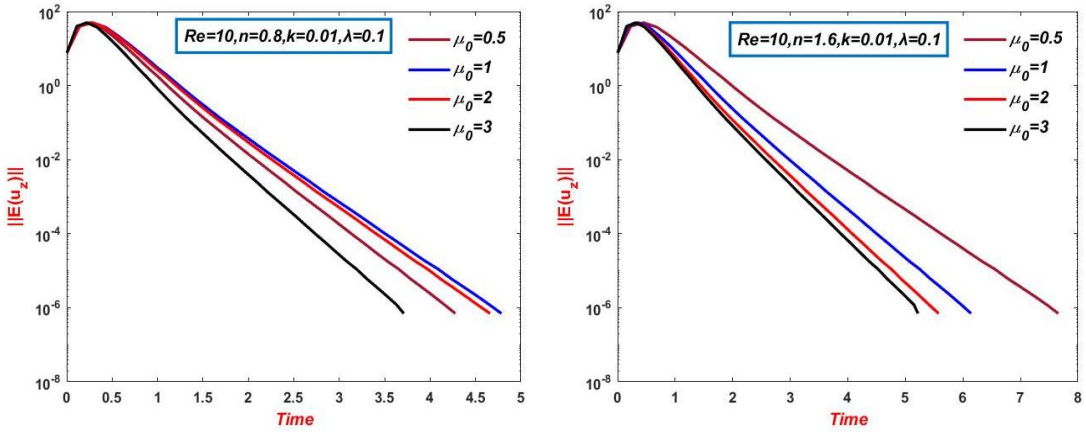

(a) (b)

Fig. 20. Convergence of velocity; μ_0-variation, *k*=0.01, *Re*=10, λ =0.1 (a) *n*=0.8, (b) *n*=1,6

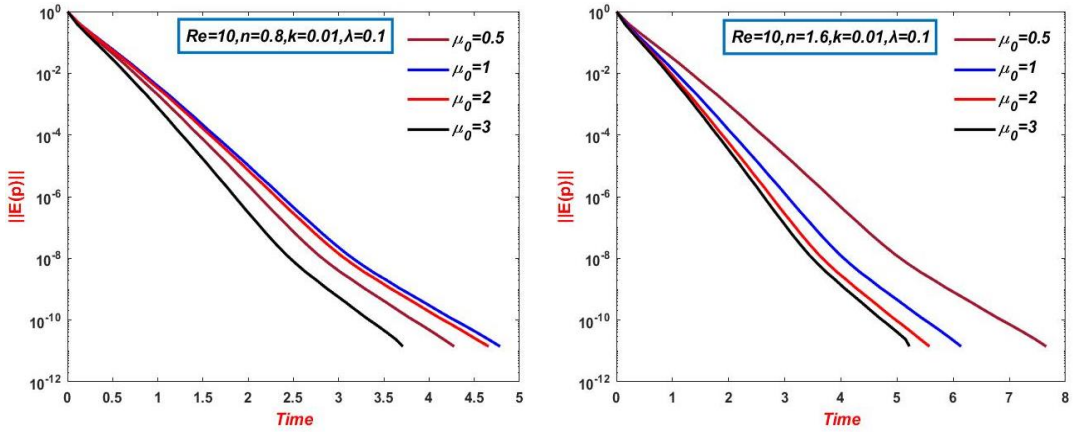

(a) (b)

Fig. 21. Convergence of pressure; μ_0-variation, *k*=0.01, *Re*=10, λ =0.1, (a) *n*=0.8, (b) *n*=1,6

4. Conclusion

This investigation covered the influence of inelastic parameters, on the convergence rate of solution components in both compounds of the shear viscosity and extensional viscosity. With the selected of shear viscosity, the effect of natural time *k* on the temporal convergence is presented, where the effect of *k* was inversely proportional to shear thickening and directly proportional to the convergence rate in shear thinning. In contrast, the power index (*n*) has an opposite convergence behavior compared to that of *k*. Furthermore, for both shear thinning and shear thickening, the zero shear viscosity μ_0 is inversely proportional to the convergence rate. The effect of Reynolds number on the level of convergence exhibits as well. In this context, the findings reveal that, the rate of convergence is reduced as *Re* reduced, which reflect an opposite feature to that of μ_0 effect in both shear thinning and shear thickening situations. For n<1 and n>1, λ direct correlates with convergence rate. Ultimately, in both shear thinning and shear thickening the effect of power index on the level of velocity and rate of convergence of solution components is presented. Here, the results show two different features, where in the shear thinning case, the level of convergence has been decreased as the values of power index (*n*) impressed. In contrast, an opposite phenomenon is occurred.

References

[1] Jamali, Muhammad Sabaruddin Ahmad, Zuhaila Ismail, and Norsarahaida Saidina Amin. "Effect of Different Types of Stenosis on Generalized Power Law Model of Blood Flow in a Bifurcated Artery." *Journal of Advanced Research in Fluid Mechanics and Thermal Sciences* 87, no. 3 (2021): 172-183. https://doi.org/10.37934/arfmts.87.3.172183

[2] Karimi, Safoora, Mahsa Dabagh, Paritosh Vasava, Mitra Dadvar, Bahram Dabir, and Payman Jalali. "Effect of rheological models on the hemodynamics within human aorta: CFD study on CT image-based geometry." *Journal of Non-Newtonian Fluid Mechanics* 207 (2014): 42-52. https://doi.org/10.1016/j.jnnfm.2014.03.007

[3] Carer, Chloé, Leonhard Xaver Driever, Stein Köbben, Max Mckenzie, Fredrik Rhenman, Onno Van de Sype, Jesse van der Toorn et al. "Effect of parameter variation on the viscosity of ethanol gel propellants." *Journal of Aerospace Technology and Management* 13 (2021). https://doi.org/10.1590/jatm.v13.1196

[4] Boyd, Joshua, James M. Buick, and Simon Green. "Analysis of the Casson and Carreau-Yasuda non-Newtonian blood models in steady and oscillatory flows using the lattice Boltzmann method." *Physics of Fluids* 19, no. 9 (2007): 093103. https://doi.org/10.1063/1.2772250

[5] Liepsch, D., S. Sindeev, and S. Frolov. "An impact of non-Newtonian blood viscosity on hemodynamics in a patient-specific model of a cerebral aneurysm." In *Journal of Physics: Conference Series*, vol. 1084, no. 1, p. 012001. IOP Publishing, 2018. https://doi.org/10.1088/1742-6596/1084/1/012001

[6] Binding, D. M., A. R. Blythe, S. Gunter, A. A. Mosquera, P. Townsend, and M. F. Webster. "Modelling polymer melt flows in wirecoating processes." *Journal of Non-Newtonian Fluid Mechanics* 64, no. 2-3 (1996): 191-206. https://doi.org/10.1016/0377-0257(96)01447-4

[7] Debbaut, B., and M. J. Crochet. "Extensional effects in complex flows." *Journal of Non-Newtonian Fluid Mechanics* 30, no. 2-3 (1988): 169-184. https://doi.org/10.1016/0377-0257(88)85023-7
[8] Mutlu, I., P. Townsend, and M. F. Webster. "Simulation of cable-coating viscoelastic flows with coupled and decoupled schemes." *Journal of Non-Newtonian Fluid Mechanics* 74, no. 1-3 (1998): 1-23. https://doi.org/10.1016/S0377-0257(97)00069-4
[9] Al-Muslimawi, Alaa Hasan A. *Numerical analysis of partial differential equations for viscoelastic and free surface flows*. Swansea University (United Kingdom), 2013.
[10] Al-Muslimawi, A., H. R. Tamaddon-Jahromi, and M. F. Webster. "Numerical simulation of tube-tooling cable-coating with polymer melts." *Korea-Australia Rheology Journal* 25 (2013): 197-216. https://doi.org/10.1007/s13367-013-0021-x
[11] Hawken, D. M., H. R. Tamaddon-Jahromi, P. Townsend, and M. F. Webster. "A Taylor-Galerkin-based algorithm for viscous incompressible flow." *International Journal for Numerical Methods in Fluids* 10, no. 3 (1990): 327-351. https://doi.org/10.1002/fld.1650100307
[12] Fadhel, Ihssan Aqeel, and Alaa Hassan Al-Muslimawi. "Simulation of Oldroyd-B Viscoelastic Fluid in Axisymmetric Straight Channel by Using a Hybrid Finite Element/Volume Method." *Journal of Advanced Research in Fluid Mechanics and Thermal Sciences* 81, no. 1 (2021): 26-40. https://doi.org/10.37934/arfmts.81.1.2640
[13] Hanafi, Hajar, and Sharidan Shafie. "Unsteady free convection MHD flow over a vertical cone in porous media with variable heat and mass flux in presence of chemical reaction." *Journal of Advanced Research in Fluid Mechanics and Thermal Sciences* 92, no. 2 (2022): 1-12. https://doi.org/10.37934/arfmts.92.2.112
[14] Xue, S-C., N. Phan-Thien, and R. I. Tanner. "Three dimensional numerical simulations of viscoelastic flows through planar contractions." *Journal of Non-Newtonian Fluid Mechanics* 74, no. 1-3 (1998): 195-245. https://doi.org/10.1016/S0377-0257(97)00072-4
[15] Kim, Ju Min, Chongyoup Kim, Jeong Ho Kim, Changkwon Chung, Kyung Hyun Ahn, and Seung Jong Lee. "High-resolution finite element simulation of 4: 1 planar contraction flow of viscoelastic fluid." *Journal of Non-Newtonian Fluid Mechanics* 129, no. 1 (2005): 23-37. https://doi.org/10.1016/j.jnnfm.2005.04.007
[16] Oliveira, Mónica SN, Paulo J. Oliveira, Fernando T. Pinho, and Manuel A. Alves. "Effect of contraction ratio upon viscoelastic flow in contractions: The axisymmetric case." *Journal of Non-Newtonian Fluid Mechanics* 147, no. 1-2 (2007): 92-108. https://doi.org/10.1016/j.jnnfm.2007.07.009
[17] Japar, Wan Mohd Arif Aziz, Nor Azwadi Che Sidik, Natrah Kamaruzaman, Yutaka Asako, and Nura Mu'az Muhammad. "Hydrothermal performance in the Hydrodynamic Entrance Region of Rectangular Microchannel Heat Sink." *Journal of Advanced Research in Numerical Heat Transfer* 1, no. 1 (2020): 22-31.
[18] Yasir, Reisan Y., Alaa H. Al-Muslimawi, and Bashaeer K. Jassim. "Numerical simulation of non-Newtonian inelastic flows in channel based on artificial compressibility method." *Journal of Applied and Computational Mechanics* 6, no. 2 (2020): 271-283.
[19] Rodríguez-Martínez, J. A., Oana Cazacu, Nitin Chandola, and Komi Espoir N'souglo. "Effect of the third invariant on the formation of necking instabilities in ductile plates subjected to plane strain tension." *Meccanica* 56 (2021): 1789-1818. https://doi.org/10.1007/s11012-021-01330-6
[20] Stavrinidis, C., J. Clinckemaillie, and J. Dubois. "New concepts for finite-element mass matrix formulations." *AIAA Journal* 27, no. 9 (1989): 1249-1255. https://doi.org/10.2514/3.10252
[21] Al-Muslimawi, Alaa H. "Taylor Galerkin pressure correction (TGPC) finite element method for incompressible Newtonian cable-coating flows." *Journal of Kufa for Mathematics and Computer* 5, no. 2 (2018). https://doi.org/10.31642/JoKMC/2018/050203
[22] Donea, Jean, and Luigi Quartapelle. "An introduction to finite element methods for transient advection problems." *Computer Methods in Applied Mechanics and Engineering* 95, no. 2 (1992): 169-203. https://doi.org/10.1016/0045-7825(92)90139-B
[23] Donea, J., S. Giuliani, H. Laval, and L. Quartapelle. "Finite element solution of the unsteady Navier-Stokes equations by a fractional step method." *Computer Methods in Applied Mechanics and Engineering* 30, no. 1 (1982): 53-73. https://doi.org/10.1016/0045-7825(82)90054-8
[24] Sharhanl, Alaa A., and Alaa Al-Muslimawi. "Numerical simulation of a power-law inelastic fluid in axisymmetric contraction by using a Taylor Galerkin-pressure correction finite element method." *International Journal of Nonlinear Analysis and Applications* 12, no. Special Issue (2021): 2211-2222.
[25] Mahmood, Rashid, Afraz Hussain Majeed, Muhammad Tahir, Imran Saddique, Nawaf N. Hamadneh, Ilyas Khan, and Asif Mehmood. "Statistical Analysis of Hydrodynamic Forces in Power-Law Fluid Flow in a Channel: Circular Versus Semi-Circular Cylinder." *Frontiers in Physics* 10 (2022): 38. https://doi.org/10.3389/fphy.2022.830408